Significant Phonon Drag Enables High Power Factor in the AlGaN/GaN Two-Dimensional Electron Gas

Ananth Saran Yalamarthy[1], Miguel Muñoz Rojo[2,3], Alexandra Bruefach[4], Derrick Boone[5,6], Karen M. Dowling[2], Peter F. Satterthwaite[2], David Goldhaber-Gordon[6,7], Eric Pop[2,8,9], and Debbie G. Senesky[2,9,10*]

[1]*Department of Mechanical Engineering, Stanford University, Stanford, CA 94305, USA.*
[2]*Department of Electrical Engineering, Stanford University, Stanford, CA 94305, USA.*
[3]*Department of Thermal and Fluid Engineering, University of Twente, Enschede, 7500 AE, Netherlands.*
[4]*Department of Materials Science and Engineering, UC Berkeley, CA 94720, USA.*
[5]*Department of Applied Physics, Stanford University, Stanford, CA 94305, USA.*
[6]*Stanford Institute for Materials and Energy Sciences, SLAC National Accelerator Laboratory, Menlo Park, CA 94025, USA.*
[7]*Department of Physics, Stanford University, Stanford, CA 94305, USA.*
[8]*Department of Materials Science and Engineering, Stanford University, Stanford, CA 94305, USA.*
[9]*Precourt Institute for Energy, Stanford University, Stanford, CA 94305, USA.*
[10]*Department of Aeronautics and Astronautics, Stanford University, Stanford, CA 94305, USA.*

**Corresponding author: Debbie G. Senesky (dsenesky@stanford.edu)*

Thermoelectric energy harvesters and sensors are based on the Seebeck effect, typically caused by diffusion of electrons or holes in a temperature gradient. However, the Seebeck effect can also have a phonon drag (PD) component, due to momentum exchange between charge carriers and lattice phonons, which is more difficult to quantify. Here, we present the first study of PD in the AlGaN/GaN two-dimensional electron gas (2DEG). We find that PD does not contribute significantly to the thermoelectric behavior of devices with ~100 nm GaN thickness, which suppress the phonon mean free path. However, when the thickness is increased to ~1.2 μm, up to 32% (88%) of the Seebeck coefficient at 300 K (50 K) can be attributed to the drag component. In turn, the PD enables state-of-the-art thermoelectric power factor in the thicker GaN film, up to ~40 mW m^{-1} K^{-2} at 50 K. By measuring the thermal conductivity of these AlGaN/GaN films, we show that the magnitude of the PD can increase even when the thermal conductivity decreases. Decoupling of thermal conductivity and Seebeck coefficient could enable important advancements in thermoelectric power conversion with devices based on 2DEGs.

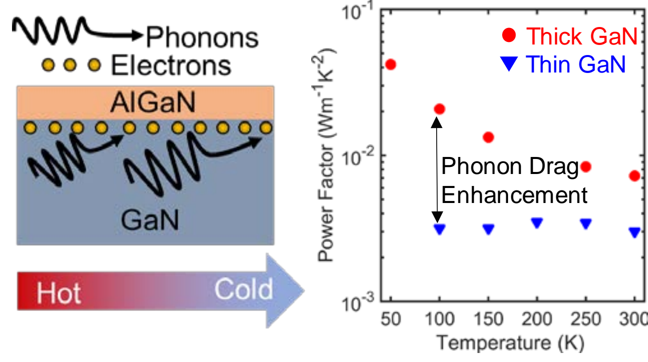

Keywords: thermoelectrics, phonon drag, 2D electron gas (2DEG), electron-phonon interaction

The scattering of electrons and holes by lattice vibrations, known as phonons, often limits the performance of modern transistors and circuits.[1] Yet that same coupling of phonons to charge carriers can also enhance the Seebeck coefficient (S), and hence allow increased power generation in thermoelectric (TE) devices.[2–4] Momentum transfer from non-equilibrium phonons to charge carriers, known as phonon drag (PD), produces a Seebeck coefficient (S_{ph}) that adds to the Seebeck coefficient from the thermal diffusion of charge carriers (S_{d}). Despite the potential gains in TE efficiency, understanding the contribution of PD to the overall Seebeck coefficient has not received much consideration, largely due to early work which suggested that: (1) S_{ph} is only significant at low temperatures ($T \leq 50$ K), where the TE power conversion efficiency (zT) is low;[5] (2) S_{ph} is small relative to S for degenerate semiconductors,[6,7] which are the most common TE materials due to their larger zT; and (3) an increase in S_{ph} coincides with a corresponding increase the thermal conductivity (k),[8–10] and thus has little benefit for power generation, because $zT \propto S^2/k$.

Contrary to these beliefs, recent experiments show that S_{ph} is almost 34% of the total S at room temperature in degenerate, bulk Si (doping of ~10^{19} cm^{-3}).[11] Further, recent first-principles calculations show that different ranges of phonon mean free paths (MFPs) contribute to thermal conductivity and PD, respectively. Remarkably, this decoupling means that k could be reduced while preserving S_{ph}.[4] This decoupling could be achieved in degenerate two-dimensional electron gases (2DEGs) in semiconductor quantum wells,[12–15] where the 2DEG is confined within a few nanometers of a surface, while the thermal conductivity k is largely determined by phonon scattering within the various layers forming the quantum well.

Previous determinations of S_{ph} in 2DEG systems have relied on measuring the total Seebeck coefficient, theoretically estimating S_{d}, and calculating $S_{\mathrm{ph}} = S - S_{\mathrm{d}}$.[16] However, estimating S_{d} is difficult, requiring precise knowledge of all scattering mechanisms, in addition

to the subband energies of the 2D quantum well. In the simple Herring model,[2] $S_{\mathrm{ph}} \propto \lambda_{\mathrm{ph}}$, where λ_{ph} is the MFP of the "representative" phonons contributing to drag. Thus, as shown in recent work on Si,[11] one can separately determine S and S_{ph} by varying the semiconductor dimensions,[17] which controls the distribution of phonon MFPs, and hence S_{ph}. As the sample thickness is reduced below a critical value, S_{ph} disappears such that in these samples $S \approx S_{\mathrm{d}}$.[11] S_{ph} in thicker samples can thus be estimated by subtracting the S_{d} of the smaller samples. Because this method does not rely on a theoretical estimate of S_{d}, it allows for a true extraction of S_{ph}, provided that the thickness reduction has minimal effect on the quantum well itself.

In this work, we extend the concept of dimension scaling to extract S_{ph} in the 2DEG that is formed at the surface of a GaN layer (of controlled thickness) capped with a thin, unintentionally doped AlGaN layer. This approach enables the first experimental measurements of S_{ph} in this material system,[4] which is possible up to room temperature given the relatively high Debye temperatures of both GaN and AlN (600 K and 1150 K).[18] In terms of potential applications, this is an appealing heterostructure for use in space environments,[19] where extreme temperature TE power sources[20] are necessary.

Experimental samples were fabricated via metal organic chemical vapor deposition (MOCVD) on a Si (111) wafer (725 μm thick, p-type, doping level of 10^{16}-10^{17} cm^{-3}), as summarized in Supplementary Figure S1. A buffer stack consisting of $Al_xGa_{1-x}N$ was grown, followed by a GaN layer whose thickness was chosen to tune the phonon scattering and confinement. Two variants were grown: (i) a "thin" sample with $t_{\mathrm{GaN}} \approx 100$ nm and (ii) a "thick" sample with $t_{\mathrm{GaN}} \approx 1.2$ μm. The 2DEG was formed by depositing 1 nm/30 nm/3 nm of AlN/$Al_{0.25}Ga_{0.75}N$/GaN (cap) on top of the GaN layer, a standard stack for achieving high electron mobility (1500 to 2000 cm^{2}V^{-1}s^{-1} at room temperature).[21] The 2DEG forms in GaN at the interface with AlGaN, with a nominal sheet density $n_{2\mathrm{D}} \approx 10^{13}$ cm^{-2} and a characteristic quantum well width of ~5 nm.[14] The GaN layer in the two variants is much larger than the quantum well width, which is necessary to ensure that its properties (such as the subband spacing and energies) are not affected. The buffer layers ($Al_xGa_{1-x}N$, $0 \leq x \leq 1$) and the GaN layer are unintentionally doped below 10^{16} cm^{-3}, ensuring that the measured Seebeck coefficient arises exclusively from the 2DEG.[22]

Extraction of TE properties (S and k_{GaN}) is facilitated by inducing a temperature gradient in the plane of the 2DEG. We accomplished this by etching the Si from the backside to create suspended AlGaN/GaN diaphragms, as depicted in Figures 1a and 1b. A 2DEG mesa

was then defined by etching off the top AlGaN except in a rectangular strip across which we measured voltage to extract the Seebeck coefficient. After forming a ~47 nm Al_2O_3 dielectric layer by atomic layer deposition (ALD) to provide electrical isolation from the 2DEG (see Supplementary Note 1), heater electrodes (Pt) were deposited to create an in-plane temperature gradient across the 2DEG mesa. A gate electrode (Au) on top of the Al_2O_3 (Figures 1a and 1c) enables modulating the charge density in the 2DEG.

Upon applying of a temperature gradient via the Pt heater, a Seebeck voltage is measured across the mesa, which is the sum of thermal diffusion of the 2DEG electrons (V_d) and the drag imparted to them by phonons in the GaN layer (V_ph), as seen in Figure 1c. Using the heater as a thermometer, we extracted the Seebeck coefficient from the voltage across the 2DEG mesa,

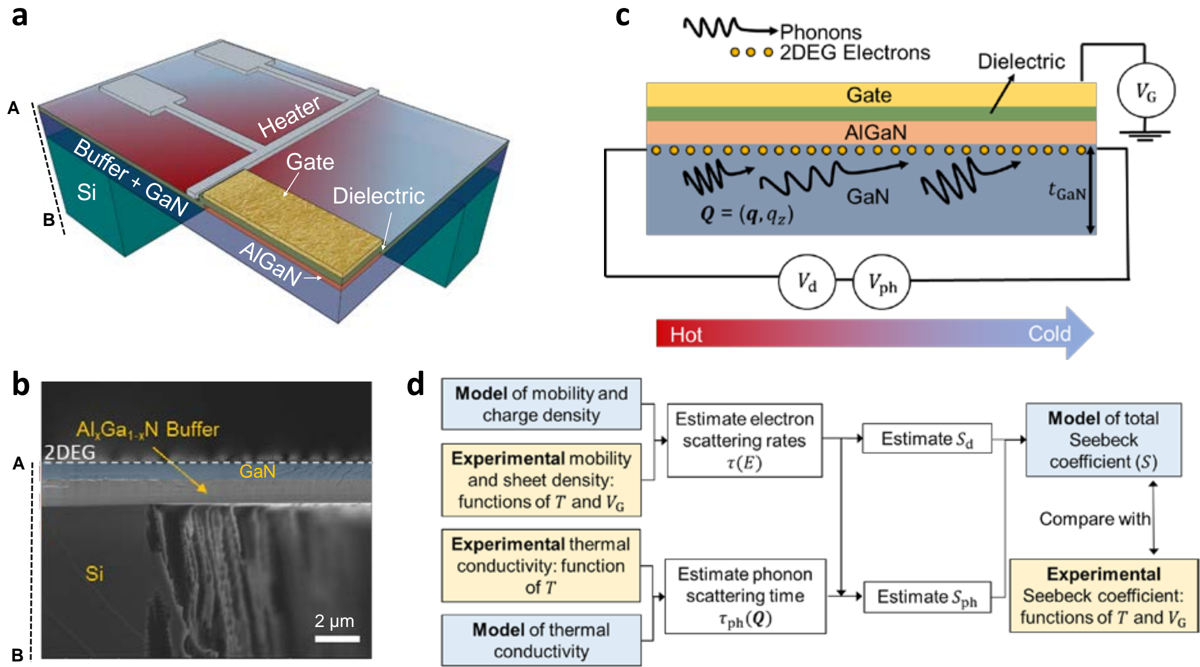

Figure 1 | Measurement platform to probe 2DEG phonon drag. (a) Schematic cross-section of suspended device to measure Seebeck coefficient, showing the heater metal, the AlGaN/GaN mesa, and the gate. (b) Cross-sectional SEM image of the suspended region, showing Si, the buffer and the GaN layer. This image is for the thick GaN sample, with $t_\mathrm{GaN} \approx 1.2$ μm. (c) 2D schematic of the suspended mesa region, showing the drag and diffusive components of the Seebeck voltage. The phonon wave vector is marked by the symbol $\boldsymbol{Q}$. (d) Flowchart showing the numerical procedure to extract the phonon drag component of the Seebeck coefficient, S_ph.

after accounting for the thermal losses in the Al_2O_3 layer and the various interfaces (see Supplementary Note 2). A similar structure with two metal electrodes (heater and sensor) on the suspended AlGaN/GaN diaphragm was used to extract the thermal conductivity of the GaN and the underlying buffer layers. Further details of the measurement process can be found in Supplementary Note 2. The flowchart in Figure 1d details our numerical procedure to extract S_ph. Measurements of the 2DEG sheet density, n_2D and mobility, μ were taken and compared

with an analytical model to obtain the energy-dependent scattering times, $\tau(E)$ for electrons in the 2DEG. The obtained $\tau(E)$ is used to calculate the diffusive component of the Seebeck coefficient, S_{d}. The thermal conductivity measurements are used to extract the energy-dependent distribution of phonon scattering lengths in the GaN layer, which is combined with $\tau(E)$ to calculate S_{ph}. This modeled S_{ph}, along with the calculated S_{d}, can be compared with the experimental values of the Seebeck coefficient for both the thick and thin GaN samples to shed light on the relative contribution of S_{ph}.

We first discuss the measurements of these parameters with the gate grounded. Figure 2a shows measurements of $n_{2\mathrm{D}}$ for the thick and thin GaN sample, extracted via Hall effect and van der Pauw measurements. The inset shows a schematic band diagram of the AlGaN/GaN

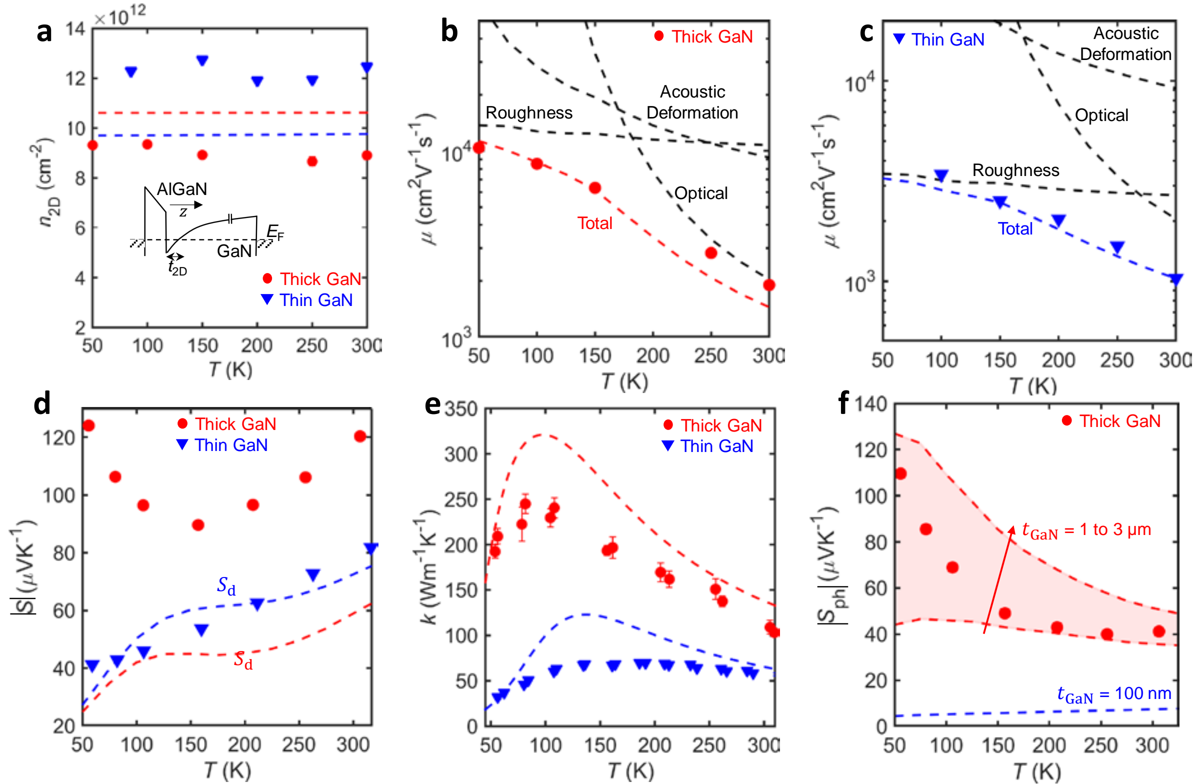

Figure 2 | Thermoelectric property measurements. (a) Temperature dependent sheet density ($n_{2\mathrm{D}}$) of the thick and thin GaN sample. The experimental markers (blue triangles and red circles) are obtained from Hall-effect and van der Pauw measurements, while the dashed lines show the simulated values obtained from a commercial solver. The inset shows a schematic of the AlGaN/GaN quantum well, with the Fermi level and the characteristic thickness of well, $t_{2\mathrm{D}}$, marked. (b,c) Mobility for the thick and thin GaN sample, with the dashed lines showing the simulated components, and the markers from Hall and van der Pauw measurements. (d) Measured Seebeck coefficient. The dashed lines show the calculated diffusive components, which are similar for the thick and thin GaN samples. (e) Measured (markers) and calculated (dashed lines) thermal conductivities for the thick and thin GaN samples. (f) Simulated values of the phonon drag component of the Seebeck coefficient obtained by sweeping the effective thickness of the GaN layer. The red markers show the estimated drag component for the thick GaN sample extracted from the experimental data. A clear suppression of phonon drag is observed for smaller GaN layer thickness.

quantum well, with the 2DEG depicted as the triangular region at the interface below the Fermi level (E_{F}). The thickness of the quantum well, $t_{2\mathrm{D}}$, is defined as the distance from the AlGaN/GaN interface to the intersection of E_F and the GaN conduction band. In both samples, we obtain sheet density $n_{2\mathrm{D}}$ roughly independent of temperature from 50 K to 300 K, consistent with the weak temperature dependence of the piezoelectric constants of both AlN and GaN.[23] The thin and thick GaN samples have a similar $n_{2\mathrm{D}} \approx 10^{13}$ cm^{-2},[14] verified using a commercially available Schrödinger-Poisson solver[24] as seen in Figure 2a. We also obtain $t_{2\mathrm{D}} \approx 6.1$ nm and $t_{2\mathrm{D}} \approx 4.4$ nm for the thick and thin GaN sample from the solver. For simplicity, in the models for TE transport properties we set $n_{2\mathrm{D}} = 10^{13}$ cm^{-2} for both samples. Using the expression for the 2D density of states, assuming that all the sheet density is from a single subband, $g_{2\mathrm{D}} = \frac{m^*}{\pi\hbar^2}$, we obtain $E_{\mathrm{F}} - E_1 \approx 110$ meV, where E_1 denotes the energy at the bottom of the first subband. Here, m^* is the electron effective mass in GaN (Table S1). This is consistent with the energies obtained from the solver (Supporting Note 3), and indicates that only the bottom subband contributes significantly to charge density. For the rest of this work, only this bottom subband is considered in the calculation of the Seebeck coefficient.[25]

Next, we turn to measurements of the 2DEG mobility obtained via Hall-effect, plotted with symbols in Figure 2b and Figure 2c for the thick and thin GaN samples, respectively. The dashed lines show the calculated contributions to the mobility from scattering mechanisms that are dominant in AlGaN/GaN 2DEGs.[26] Other scattering mechanisms (e.g. dislocation, ionized impurity and piezoelectric scattering) are neglected. Rigorous justification of this approximation is found in Supplementary Note 2. For both thick and thin GaN, polar optical phonon (POP) scattering is the dominant scattering mechanism at room temperature, due to the large optical phonon energy ($\hbar\omega_{\mathrm{OP}} = 91.2$ meV),[27] and the polar nature[28] of the GaN wurtzite crystal. Though the optical phonon population decreases exponentially at lower temperatures, electrons in the lower subband still scatter against the AlGaN/GaN interface roughness. To estimate this component, we set the root-mean-square (RMS) roughness height, $\Delta = 1$ and 2 nm for the thick and thin GaN sample, respectively (atomic force microscopy of the sample surface can be found in Supplementary Figure S4). The good agreement between the model and experimental data allows us to extract the energy-dependent scattering time, $\tau(E)$ for electrons in the bottom subband of the 2DEG.

From this, we can calculate the diffusive component of the Seebeck coefficient for the bottom subband[29]

$$S_{\mathrm{d}} = \frac{-1}{eT} \frac{\int E \frac{\partial f_0(E)}{\partial E} (E - E_{\mathrm{F}} - E_1) \tau(E) dE}{\int E \frac{\partial f_0(E)}{\partial E} \tau(E) dE}, \tag{1}$$

where $f_0(E)$ is the equilibrium Fermi function, and e is the magnitude of the electronic charge. These are plotted against the experimental data for the magnitude of the Seebeck coefficient (the actual sign is negative) in Figure 2d. The theoretical curves deviate slightly from a linear dependence on temperature, typical for a degenerate semiconductor.[25] This deviation is due to POP scattering, which forbids electrons with energies smaller than $\hbar\omega_{\mathrm{OP}}$ from emitting optical phonons.[29] The slight difference in the calculated values of S_{d} for the thick and thin GaN sample is found to arise from the difference in the roughness scattering component of $\tau(E)$. We observe that the Seebeck coefficient for the thin GaN sample agrees well with the calculated S_{d}, however this model cannot describe the thick GaN sample (Figure 2d). In addition, the magnitude of the Seebeck coefficient in the thick GaN sample exhibits a prominent upturn at low temperatures, hinting at PD.[16]

In our device, three-dimensional (3D) phonons, represented by the wave vector $\boldsymbol{Q} = (\boldsymbol{q}, q_{\mathrm{z}})$, which represent the in-plane (of the 2DEG) and out-of-plane component, scatter with 2D electrons in the bottom subband, giving rise to S_{ph}. To calculate this drag, we follow the approach introduced by Cantrell and Butcher[3] and later modified by Smith.[30,31] We explicitly include the dependence of phonon scattering time (τ_{ph}) on the phonon wave vector

$$S_{\mathrm{ph}} = -\frac{(2m^*)^{\frac{3}{2}} v_{\mathrm{av}}^2}{4(2\pi)^3 k_{\mathrm{B}} T^2 n_{\mathrm{2D}} e \rho} \int_0^{\infty} dq \int_{-\infty}^{\infty} dq_z \frac{\Xi^2(\boldsymbol{Q}) q^2 Q^2 |I(q_z)|^2 G(\boldsymbol{Q}) \tau_{\mathrm{ph}}(\boldsymbol{Q})}{S^2(q,T) \sinh^2\left(\frac{\hbar\omega_Q}{2k_{\mathrm{B}}T}\right)}. \tag{2}$$

In Equation 2, v_{av} is the average phonon velocity over the different modes, k_{B} is the Boltzmann constant, and ρ is the mass density of GaN. Values of the parameters used for our calculations are in Supplementary Table S1. The phonon frequency, ω_Q is approximated as $v_{\mathrm{av}}\sqrt{q^2 + q_z^2}$ assuming a 3D isotropic linear dispersion. The term $I(q_z) = \int \psi(z)^2 e^{iq_z z}$ describes the electron-phonon momentum conservation in the z direction, where $\psi(z)$ is the wave function of the electrons in the bottom subband. $\Xi(\boldsymbol{Q})$ represents the strength of the electron-phonon coupling. The terms $S(q,T)$ and $G(\boldsymbol{Q})$ represent a screening function for the electrons and an energy integral, respectively (the detailed explanation of these terms is discussed in Supplementary Note 4). Of particular interest to this work is $\tau_{\mathrm{ph}}(\boldsymbol{Q})$, representing the phonon

relaxation time. This term describes the scaling dependence of S_{ph} on sample thickness, because $\tau_{\mathrm{ph}}(\boldsymbol{Q}) \propto t_{\mathrm{GaN}}$ due to boundary scattering.

To calculate $\tau_{\mathrm{ph}}(\boldsymbol{Q})$ accurately, we measured the thermal conductivity, k, of the suspended diaphragms, presented in Figure 2e. Because our suspended film is a composite consisting of an AlN layer, $Al_xGa_{1-x}N$ transition layers and a GaN layer, the overall thermal conductivity must be estimated from an average of the thermal conductivities, weighted by the thicknesses of individual layers. For each layer, we used a Boltzmann Transport Equation (BTE) model to quantify its thermal conductivity. The dashed lines in Figure 2e show the modeled k for the entire stack, taking into account phonon-phonon, dislocation, alloy and boundary scattering using standard values of the elastic moduli for AlN and GaN (details in Supplementary Note 5). This use of standard values of the elastic moduli, alloy scattering, and dislocation scattering terms, which are challenging to obtain experimentally,[32,33] could explain the disagreement between the model and the data at the lower temperatures. Yet, this model will suffice to explain the observed trends in the PD behavior. Assuming that only the phonons in the GaN layer contribute to drag, the modelled τ_{ph} for this layer is combined with Equation 2 to calculate S_{ph}.

The modeled $|S_{\mathrm{ph}}|$ is plotted in Figure 2f for a range of t_{GaN} values. The magnitude of S_{ph} (actually negative in sign) for the thin GaN is between 4 and 8 μVK^{-1} across all T, significantly less than the measured 40 to 80 μVK^{-1} (Figure 2d), supporting the conclusion that $S \approx S_{\mathrm{d}}$. The near temperature-independence of the modeled S_{ph} is due to k_{GaN} being limited by boundary scattering across the entire temperature range. S_{ph} in the thick GaN film was estimated by subtracting a linear fit (including the origin) of the measured Seebeck coefficient in the thin GaN sample from the measured Seebeck coefficient of the thick GaN sample. We have used a linear fit including the origin of the thin GaN Seebeck coefficient to avoid overestimating the diffusive component of the Seebeck coefficient. This is because the measured Seebeck coefficient values of the thin GaN sample still includes a small PD component, which is visible as a slight flattening at the lower temperatures (blue triangles in Figure 2d).

The estimate of S_{ph} for the thick GaN sample after subtraction from the linear fit is plotted in Figure 2f (red markers). The shaded region shows the calculated S_{ph} for various effective GaN thicknesses (t_{GaN}) from 1 to 3 μm using Equation 2. We have swept the GaN thickness in the model because it under-predicts S_{ph} if we use the actual thickness (1.2 μm).

This inaccuracy may arise from the simple model for the thermal conductivity and PD used here, and the difficulty in determining the 2DEG quantum well thickness experimentally. The data and model exhibit the correct trend within the swept thickness range. The experimental S_{ph} data (red circles in Figure 2f) show that ~32% of the total S at room temperature can be attributed to drag, increasing to almost 88% of S at 50 K for the thick GaN sample. The inverse temperature dependence of S_{ph} is reflective of phonon-phonon scattering, from which the phonon MFP scales as T^{-1}. The measurements of the Seebeck coefficient and the thermal conductivity for the thick GaN sample below ~90 K (red circles) in Figures 2e and 2f also suggest that the PD continues to increase even when the thermal conductivity starts decreasing. This provides experimental evidence that these two parameters can be decoupled to increase zT, in agreement with previous theoretical work.[34,35]

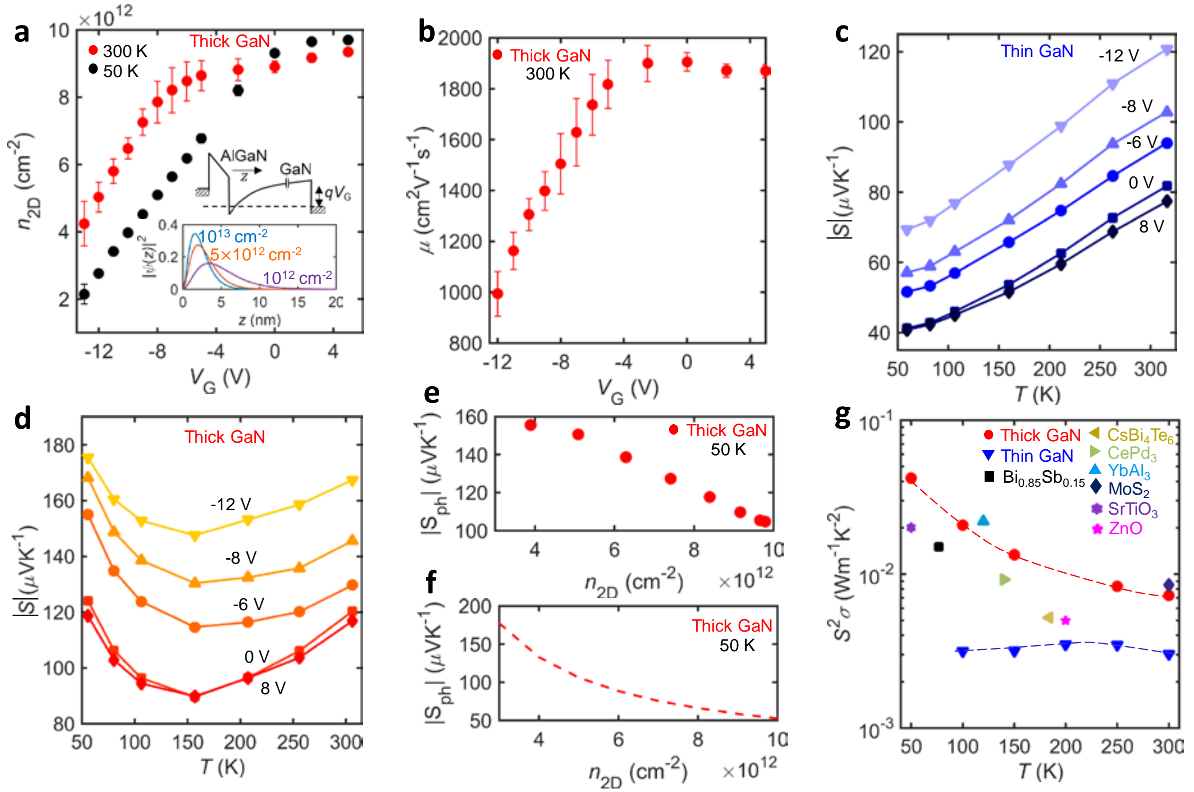

Figure 3 | Measurements with a gate bias. (a) Modulation of the sheet density in the 2DEG (n_{2D}) with applied gate bias at 300 K and 50 K for the thick GaN sample. The markers are obtained from Hall-effect measurements. The inset shows the simulated wave function in the bottom subband of the 2DEG for three different sheet densities. The coordinate z=0 corresponds to the AlGaN/GaN interface, as seen in the band diagram (black lines). Positive z represents the GaN layer. (b) Experimental measurements of field-effect mobility at 300 K. (c,d) Gated Seebeck coefficient measurements for the thin and thick GaN sample. The solid lines are a guide for the eye, while the makers are the experimental measurements. (e) Estimated drag component for the thick GaN sample from the experimental data, at 50 K. (f) Simulated phonon drag component for the thick GaN sample (using t_{GaN} = 1.2 μm) for 2DEG sheet densities that correspond to our applied voltage range, at 50 K. (g) Estimated temperature-

dependent power factors for the thin and the thick GaN samples from 50 to 300 K from the experimental data, with the gate grounded. The dashed red and blue lines are guidelines for the eye. We have also included power factor data from other material systems for comparison with the thick GaN 2DEG.

The application of a gate voltage, V_{G}, can tune the TE power factor ($S^2\sigma$) without changing k, which can further optimize zT.[36,37] While the effect of V_{G} on S_{d} is well known, only a few studies have attempted to quantify its effect on drag.[16,38,39] In particular, application of V_{G} tunes the quantum well width and 2DEG charge density (n_{2D}), simultaneously. S_{ph} is inversely proportional to n_{2D} giving it a strong dependency on this parameter, as seen in Equation 2. Quantum well width affects S_{ph} through $I(q_z)$ which is strongly dependent on the wave function $\psi(z)$. A more tightly confined wave function in real space (which corresponds to larger n_{2D}) is broader in Fourier space, increasing $I(q_z)$. These two effects compete against each other, resulting in a complex gate voltage dependency.

Hall-effect measurements of the 2DEG sheet density as a function of gate voltage are presented in Figure 3a. The data at 300 K shows a depletion of the 2DEG sheet density by up to a factor of ~3x from its ungated value as V_{G} is lowered to -12 V. The gating is similar at lower temperatures (data for the thick GaN sample at 50 K are plotted with black circles in Figure 3a) and for the thin GaN sample. The inset of Figure 3a shows how depletion widens the quantum well at the AlGaN/GaN interface. Depletion also reduces the 2DEG mobility as seen in Figure 3b, similar to former work.[40,41] To study the effect of gating on S_{ph}, we need to first estimate S_{d} as a function of gate voltage. This can be done by studying the effect of V_{G} on the thin GaN sample, presented in Figure 3c. For a degenerate 2D quantum well, we can roughly approximate the magnitude diffusive Seebeck coefficient as $S_{\mathrm{d}} \propto T/(E_{\mathrm{F}} - E_1)$.[25] Since $n_{\mathrm{2D}} \propto (E_{\mathrm{F}} - E_1)$, the magnitude of the diffusive Seebeck coefficient should increase as negative V_{G} depletes the 2DEG, and decrease linearly with T. Both features are visible in Figure 3c.

Figure 3d shows the effect of V_{G} on |S| in the thick GaN sample, where the upturn below ~150 K is apparent even after depletion. As in Figure 2f, we subtracted a linear fit of the thin GaN Seebeck coefficients (in Figure 3c) from the values for the thick GaN to estimate S_{ph} for different V_{G}. Because we know the relation between n_{2D} and V_{G} (Figure 3a), we can thus estimate S_{ph} as a function of n_{2D}. We have plotted the gate-voltage dependence of S_{ph} at a fixed temperature of 50 K, for different n_{2D} values in Figure 3e. It is seen that $|S_{\mathrm{ph}}|$ increases by a factor of ~1.5x as n_{2D} decreases from 10^{13} cm^{-2} to 3×10^{12} cm^{-2}. To confirm the trend of these values, we also simulated S_{ph} over this n_{2D} range using Equation 2 (with the actual GaN thickness of 1.2 μm), taking into account the shape of the quantum well. These simulations are

plotted in Figure 3f at a temperature of 50 K, for ease of comparison to the data in Figure 3e. The simulated data shows the same trend (i.e., $|S_{\mathrm{ph}}|$ increasing as $n_{2\mathrm{D}}$ decreases), but the increase is much larger (~3x). Although the reason for the mismatch needs further study, these trends of $\mathrm{S_{ph}}$ vs. V_{G} suggest that the Seebeck coefficient behavior in the thick GaN sample is indeed due to PD. Further, they show that depleting the AlGaN/GaN 2DEG increases the magnitudes of both the diffusive and drag components of the Seebeck coefficient.

Finally, it is worthwhile to examine the TE power factor ($S^2\sigma$) of the 2DEG in both the thick and the thin GaN sample. These values are plotted in Figure 3g, where the gate is grounded. In order to calculate the conductivity of the 2DEG, σ, we use the mobility values in Figure 2b and Figure 2c, along with an estimate for the average volumetric charge density, $n_{\mathrm{v}} = n_{2\mathrm{D}}/t_{2\mathrm{D}}$.[41] The $n_{2\mathrm{D}}$ values are taken from the experimental values in Figure 2a. While the power factor for the thin GaN sample is quite insensitive to temperature, the value for the thick GaN sample shows a pronounced enhancement at low temperatures, as seen in Figure 3g, reaching ~40 mW m^{-1} K^{-2} at 50 K. This high power factor, which originates from the upturn of the Seebeck coefficient at low temperatures via PD, is state-of-the-art when compared with other TE materials also plotted in Figure 3g ($Bi_{0.85}Sb_{0.15}$,[42] $CsBi_4Te_6$,[43] $CePd_3$,[44] $YbAl_3$,[45] MoS_2[46]). We have also plotted the power factors for other 2DEG systems where measurements are available, such as gated ZnO[37] and gated $SrTiO_3$[38] for comparison in Figure 3g. The enhancement of the Seebeck coefficient in our thick GaN sample is in contrast with typical TE materials, where the power factor scales directly with temperature because the Seebeck coefficient is diffusive.[43] The high power factor values in the thick GaN sample, although only for a single 2DEG, are promising for planar applications such as Peltier coolers. Further, they could make promising low-temperature energy harvesting elements when structured as a superlattice.[47]

In conclusion, we have experimentally shown that PD can be a significant portion of the total Seebeck coefficient in a 2DEG, even at room temperature. By using thickness as a “knob” to control sample dimensions, we show that S_{ph} is suppressed in the AlGaN/GaN 2DEG at a film thickness of ~100 nm. From a TE power conversion perspective, we shed light on two important phenomena: First, the magnitude of the PD can increase even when the thermal conductivity is decreasing, which means that these could be tuned separately. Second, depleting a 2DEG can lead to an increase in both the PD and diffusive contributions of the Seebeck coefficient. These findings enable a better understanding of the PD effect, and can lead to advancements in TE power conversion across a wide range of temperatures.

Acknowledgements

This work was supported in part by the National Science Foundation (NSF) Engineering Research Center for Power Optimization of Electro Thermal Systems (POETS) under Grant EEC-1449548, and by the NSF DMREF grant 1534279. The MOCVD experiments were conducted at the MOCVD Lab of the Stanford Nanofabrication Facility (SNF), which is partly supported by the NSF as part of the National Nanotechnology Coordinated Infrastructure (NNCI) under award ECCS-1542152. Hall measurements were supported by the U.S. Department of Energy, Office of Science, Basic Energy Sciences, Materials Sciences and Engineering Division, under Contract DE-AC02-76SF00515. D.B.'s participation in this research was facilitated in part by a National Physical Science Consortium Fellowship and by stipend support from the National Institute of Standards and Technology.

References

(1) Pop, E. Energy Dissipation and Transport in Nanoscale Devices. *Nano Res.* **2010**, *3* (3), 147–169. https://doi.org/10.1007/s12274-010-1019-z.

(2) Herring, C. Theory of the Thermoelectric Power of Semiconductors. *Phys. Rev.* **1954**, *96* (5), 1163–1187. https://doi.org/10.1103/PhysRev.96.1163.

(3) Cantrell, D. G.; Butcher, P. N. A Calculation of the Phonon-Drag Contribution to the Thermopower of Quasi-2D Electrons Coupled to 3D Phonons. 1. General Theory. *J. Phys. C* **1987**, *20* (1985).

(4) Zhou, J.; Liao, B.; Qiu, B.; Huberman, S.; Esfarjani, K.; Dresselhaus, M. S.; Chen, G. Ab Initio Optimization of Phonon Drag Effect for Lower-Temperature Thermoelectric Energy Conversion. *Proc. Natl. Acad. Sci.* **2015**, *112* (48), 14777–14782. https://doi.org/10.1073/pnas.1512328112.

(5) Geballe, T. H.; Hull, G. W. Seebeck Effect in Germanium. *Phys. Rev.* **1954**, *94* (5), 1134–1140. https://doi.org/10.1103/PhysRev.94.1134.

(6) Weber, L.; Gmelin, E. Transport Properties of Silicon. *Appl. Phys. A* **1991**, *53*, 136–140. https://doi.org/10.1007/BF00323873.

(7) Conwell, E.; Weisskopf, V. F. Theory of Impurity Scattering in Semiconductors. *Phys. Rev.* **1950**, *77* (3), 388–390. https://doi.org/10.1103/PhysRev.77.388.

(8) Wang, G.; Endicott, L.; Chi, H.; Los, P. Tuning the Temperature Domain of Phonon Drag in Thin Films by the Choice of Substrate. *Phys. Rev. Lett.* **2013**, *111* (4), 046803.

https://doi.org/10.1103/PhysRevLett.111.046803.

(9) Takahashi, H.; Okazaki, R.; Ishiwata, S.; Taniguchi, H.; Okutani, A.; Hagiwara, M.; Terasaki, I. Colossal Seebeck Effect Enhanced by Quasi-Ballistic Phonons Dragging Massive Electrons in $FeSb_2$. *Nat. Commun.* **2016**, *7*, 12732. https://doi.org/10.1038/ncomms12732.

(10) Koirala, M.; Wang, H.; Pokharel, M.; Yucheng, L.; Chuanfei, G.; Opeil, C.; Ren, Z. Nanostructured $YbAgCu_4$ for Potentially Cryogenic Thermoelectric Cooling. *Nano Lett.* **2014**, *14* (9), 5016–5020.

(11) Sadhu, J.; Tian, H.; Ma, J.; Azeredo, B.; Kim, J.; Balasundaram, K.; Zhang, C.; Li, X.; Ferreira, P. M.; Sinha, S. Quenched Phonon Drag in Silicon Nanowires Reveals Significant Effect in the Bulk at Room Temperature. *Nano Lett.* **2015**, *15* (5), 3159–3165. https://doi.org/10.1021/acs.nanolett.5b00267.

(12) Ohta, H.; Kim, S.; Mune, Y.; Mizoguchi, T.; Nomura, K.; Ohta, S.; Nomura, T.; Nakanishi, Y.; Ikuhara, Y.; Hirano, M.; et al. Giant Thermoelectric Seebeck Coefficient of a Two-Dimensional Electron Gas in SrTiO3. *Nat. Mater.* **2007**, *6* (2), 129–134. https://doi.org/10.1038/nmat1821.

(13) Zhang, Y.; Feng, B.; Hayashi, H.; Chang, C.-P.; Sheu, Y.-M.; Tanaka, I.; Ikuhara, Y.; Ohta, H. Double Thermoelectric Power Factor of a 2D Electron System. *Nat. Commun.* **2018**, *9* (1), 2224. https://doi.org/10.1038/s41467-018-04660-4.

(14) Yalamarthy, A. S.; So, H.; Muñoz Rojo, M.; Suria, A. J.; Xu, X.; Pop, E.; Senesky, D. G. Tuning Electrical and Thermal Transport in AlGaN/GaN Heterostructures via Buffer Layer Engineering. *Adv. Funct. Mater.* **2018**, *28* (22), 1705823. https://doi.org/10.1002/adfm.201705823.

(15) Sztein, A.; Bowers, J. E.; DenBaars, S. P.; Nakamura, S. Polarization Field Engineering of GaN/AlN/AlGaN Superlattices for Enhanced Thermoelectric Properties. *Appl. Phys. Lett.* **2014**, *104* (4), 042106. https://doi.org/10.1063/1.4863420.

(16) Pallecchi, I.; Telesio, F.; Marré, D.; Li, D.; Gariglio, S.; Triscone, J. M.; Filippetti, A. Large Phonon-Drag Enhancement Induced by Narrow Quantum Confinement at the $LaAlO_3/SrTiO_3$ Interface. *Phys. Rev. B* **2016**, *93* (19), 195309. https://doi.org/10.1103/PhysRevB.93.195309.

(17) Pokharel, M.; Zhao, H.; Lukas, K.; Ren, Z.; Opeil, C.; Mihaila, B. Phonon Drag Effect in Nanocomposite $FeSb_2$. *MRS Commun.* **2013**, *3* (1), 31–36. https://doi.org/10.1557/mrc.2013.7.

(18) Sztein, A.; Haberstroh, J.; Bowers, J. E.; DenBaars, S. P.; Nakamura, S. Calculated

Thermoelectric Properties of $In_xGa_{1-x}N$, $In_xAl_{1-x}N$, and $Al_xGa_{1-x}N$. *J. Appl. Phys.* **2013**, *113* (18), 183707. https://doi.org/10.1063/1.4804174.

(19) Mishra, U. K.; Parikh, P.; Wu, Y. F. AlGaN/GaN HEMTs - An Overview of Device Operation and Applications. *Proc. IEEE* **2002**, *90* (6), 1022–1031. https://doi.org/10.1109/JPROC.2002.1021567.

(20) Yang, J.; Caillat, T. Thermoelectric Materials for Space. *MRS Bull.* **2006**, *31* (March), 224–229.

(21) Smorchkova, I. P.; Chen, L.; Mates, T.; Shen, L.; Heikman, S.; Moran, B.; Keller, S.; DenBaars, S. P.; Speck, J. S.; Mishra, U. K. AlN/GaN and (Al,Ga)N/AlN/GaN Two-Dimensional Electron Gas Structures Grown by Plasma-Assisted Molecular-Beam Epitaxy. *J. Appl. Phys.* **2001**, *90* (10), 5196–5201. https://doi.org/10.1063/1.1412273.

(22) Bahk, J.; Favaloro, T.; Shakouri, A. Thin Film Thermoelectric Characterization Techniques. *Annu. Rev. Heat Transf.* **2013**, *16* (30), 51. https://doi.org/10.1615/AnnualRevHeatTransfer.v16.30.

(23) Ambacher, O.; Majewski, J.; Miskys, C.; Link, A.; Hermann, M.; Eickhoff, M.; Stutzmann, M.; Bernardini, F.; Fiorentini, V.; Tilak, V.; et al. Pyroelectric Properties of Al(In)GaN/GaN Hetero- and Quantum Well Structures. *J. Phys. Condens. Matter* **2002**, *14* (13), 3399–3434. https://doi.org/10.1088/0953-8984/14/13/302.

(24) Birner, S.; Zibold, T.; Andlauer, T.; Kubis, T.; Sabathil, M.; Trellakis, A.; Vogl, P. Nextnano : General Purpose 3-D Simulations. *IEEE Trans. Electron Devices* **2007**, *54* (9), 2137–2142.

(25) Pallecchi, I.; Codda, M.; Galleani D'Agliano, E.; Marré, D.; Caviglia, A. D.; Reyren, N.; Gariglio, S.; Triscone, J. M. Seebeck Effect in the Conducting $LaAlO_3/SrTiO_3$ Interface. *Phys. Rev. B* **2010**, *81* (8), 085414. https://doi.org/10.1103/PhysRevB.81.085414.

(26) Gurusinghe, M. N.; Davidsson, S. K.; Andersson, T. G. Two-Dimensional Electron Mobility Limitation Mechanisms in $Al_xGa_{1-x}N/GaN$ Heterostructures. *Phys. Rev. B* **2005**, *72* (4), 045316. https://doi.org/10.1103/PhysRevB.72.045316.

(27) Foutz, B. E.; O'Leary, S. K.; Shur, M. S.; Eastman, L. F. Transient Electron Transport in Wurtzite GaN, InN, and AlN. *J. Appl. Phys.* **1999**, *85* (11), 7727–7734. https://doi.org/10.1063/1.370577.

(28) Ambacher, O.; Foutz, B.; Smart, J.; Shealy, J. R.; Weimann, N. G.; Chu, K.; Murphy, M.; Sierakowski, A. J.; Schaff, W. J.; Eastman, L. F.; et al. Two Dimensional Electron Gases Induced by Spontaneous and Piezoelectric Polarization in Undoped and Doped

AlGaN/GaN Heterostructures. *J. Appl. Phys.* **2000**, *87* (1), 334–344. https://doi.org/10.1063/1.371866.

(29) Davoody, A. H.; Ramayya, E. B.; Maurer, L. N.; Knezevic, I. Ultrathin GaN Nanowires: Electronic, Thermal, and Thermoelectric Properties. *Phys. Rev. B* **2014**, *89* (11), 115313. https://doi.org/10.1103/PhysRevB.89.115313.

(30) Fletcher, R.; Pudalov, V.; Feng, Y.; Tsaousidou, M.; Butcher, P. N. Thermoelectric and Hot-Electron Properties of a Silicon Inversion Layer. *Phys. Rev. B* **1997**, *56* (19), 12422–12428. https://doi.org/10.1103/PhysRevB.56.12422.

(31) Sankeshwar, N. S.; Kamatagi, M. D.; Mulimani, B. G. Behaviour of Diffusion Thermopower in Bloch-Grüneisen Regime in AlGaAs/GaAs and AlGaN/GaN Heterostructures. *Phys. status solidi* **2005**, *242* (14), 2892. https://doi.org/10.1002/pssb.200441177.

(32) Liu, W.; Balandin, A. A. Thermal Conduction in $Al_xGa_{1-x}N$ Alloys and Thin Films. *J. Appl. Phys.* **2005**, *97* (7), 073710. https://doi.org/10.1063/1.1868876.

(33) Zou, J.; Kotchetkov, D.; Balandin, A. A.; Florescu, D. I.; Pollak, F. H. Thermal Conductivity of GaN Films: Effects of Impurities and Dislocations. *J. Appl. Phys.* **2002**, *92* (5), 2534–2539. https://doi.org/10.1063/1.1497704.

(34) Poudel, B.; Hao, Q.; Ma, Y.; Lan, Y.; Minnich, A.; Yu, B.; Yan, X.; Wang, D.; Muto, A.; Vashaee, D.; et al. High-Thermoelectric Performance of Nanostructured Bismuth Antimony Telluride Bulk Allys. *Sci.* **2008**, *320* (5876), 634–638. https://doi.org/10.1126/science.1155140.

(35) Tian, Z.; Lee, S.; Chen, G. Heat Transfer in Thermoelectric Materials and Devices. *J. Heat Transfer* **2013**, *135* (6), 061605. https://doi.org/10.1115/1.4023585.

(36) Ryu, H. J.; Aksamija, Z.; Paskiewicz, D. M.; Scott, S. A.; Lagally, M. G.; Knezevic, I.; Eriksson, M. A. Quantitative Determination of Contributions to the Thermoelectric Power Factor in Si Nanostructures. *Phys. Rev. Lett.* **2010**, *105* (25), 15–18. https://doi.org/10.1103/PhysRevLett.105.256601.

(37) Shimizu, S.; Bahramy, M. S.; Iizuka, T.; Ono, S.; Miwa, K.; Tokura, Y.; Iwasa, Y. Enhanced Thermopower in ZnO Two-Dimensional Electron Gas. *Proc. Natl. Acad. Sci.* **2016**, *113* (23), 6438–6443. https://doi.org/10.1073/pnas.1525500113.

(38) Shimizu, S.; Ono, S.; Hatano, T.; Iwasa, Y.; Tokura, Y. Enhanced Cryogenic Thermopower in $SrTiO_3$ by Ionic Gating. *Phys. Rev. B* **2015**, *92* (16), 165304. https://doi.org/10.1103/PhysRevB.92.165304.

(39) Pallecchi, I.; Telesio, F.; Li, D.; Fête, A.; Gariglio, S.; Triscone, J. M.; Filippetti, A.;

Delugas, P.; Fiorentini, V.; Marré, D. Giant Oscillating Thermopower at Oxide Interfaces. *Nat. Commun.* **2015**, *6*, 6678. https://doi.org/10.1038/ncomms7678.

(40) Antoszewski, J.; Gracey, M.; Dell, J. M.; Faraone, L.; Fisher, T. A.; Parish, G.; Wu, Y. F.; Mishra, U. K. Scattering Mechanisms Limiting Two-Dimensional Electron Gas Mobility in $Al_{0.25}Ga_{0.75}N$/GaN Modulation-Doped Field-Effect Transistors. *J. Appl. Phys.* **2000**, *87* (8), 3900–3904. https://doi.org/10.1063/1.372432.

(41) Ohta, H.; Kim, S. W.; Kaneki, S.; Yamamoto, A.; Hashizume, T. High Thermoelectric Power Factor of High-Mobility 2D Electron Gas. *Adv. Sci.* **2017**, 1700696. https://doi.org/10.1002/advs.201700696.

(42) Yim, W. M.; Amith, A. BiSb Alloys for Magneto-Thermoelectric and Thermomagnetic Cooling. *Solid State Electron.* **1972**, *15* (10), 1141–1165. https://doi.org/10.1016/0038-1101(72)90173-6.

(43) Chung, D. Y.; Hogan, T. P.; Rocci-Lane, M.; Brazis, P.; Ireland, J. R.; Kannewurf, C. R.; Bastea, M.; Uher, C.; Kanatzidis, M. G. A New Thermoelectric Material: $CsBi_4Te_6$. *J. Am. Chem. Soc.* **2004**, *126* (20), 6414–6428. https://doi.org/10.1021/ja039885f.

(44) Gambino, R. J.; Grobman, W. D.; Toxen, A. M. Anomalously Large Thermoelectric Cooling Figure of Merit in the Kondo Systems $CePd_3$ and $CeIn_3$. *Appl. Phys. Lett.* **1973**, *22* (10), 506–507. https://doi.org/10.1063/1.1654486.

(45) Van Daal, H. J.; Van Aken, P. B.; Buschow, K. J. H. The Seebeck Coefficient of $YbAl_2$ and $YbAl_3$. *Phys. Lett. A* **1974**, *49* (3), 49–51.

(46) Hippalgaonkar, K.; Wang, Y.; Ye, Y.; Qiu, D. Y.; Zhu, H.; Wang, Y.; Moore, J.; Louie, S. G.; Zhang, X. High Thermoelectric Power Factor in Two-Dimensional Crystals of MoS_2. *Phys. Rev. B* **2017**, *95* (11), 115407. https://doi.org/10.1103/PhysRevB.95.115407.

(47) Sztein, A.; Bowers, J. E.; Denbaars, S. P.; Nakamura, S. Polarization Field Engineering of GaN / AlN / AlGaN Superlattices for Enhanced Thermoelectric Properties. *Appl. Phys. Lett.* **2014**, *042106*. https://doi.org/10.1063/1.4863420.